Complex Kinetics of the Electron Transfer between the Photoactive Redox Label TUPS and the Heme of Cytochrome c

Katalin Tenger,[†] Petro Khoroshyy,[†] Balázs Leitgeb,[†] Gábor Rákhely,[†,‡] Natalia Borovok,[§] Alexander Kotlyar,[§] Dmitry A. Dolgikh,[||] and László Zimányi*,[†]

Institute of Biophysics, Biological Research Center of the Hungarian Academy of Sciences, Szeged, Hungary, Department of Biotechnology, University of Szeged, Szeged, Hungary, Department of Biochemistry, George S. Wise Faculty of Life Sciences, Tel Aviv University, Ramat Aviv, Israel, and Institute of Bioorganic Chemistry, Russian Academy of Sciences, Moscow, Russia

Received May 2, 2005

The photoinduced covalent redox label 8-thiouredopyrene-1,3,6-trisulfonate (TUPS) has been attached to two lysine residues (K8 and K39) at opposite sides of horse heart cytochrome c, as well as to cysteines, at the same positions, introduced by site-directed mutagenesis. Electron transfer between TUPS and the heme of cytochrome c deviates from the expected monoexponential kinetic behavior. Neither the overall rate nor the individual exponential components of electron transfer, as followed by kinetic absorption spectroscopy, correlate with the length of the covalent link connecting the dye with the protein. Molecular dynamics calculations show that TUPS can approach the protein surface and occupy several such positions. This heterogeneity may explain the multiexponential electron-transfer kinetics. The calculated optimal electron-transfer pathways do not follow the covalent link but involve through space jumps from the dye to the protein moiety, effectively decoupling the length of the covalent link and the electron-transfer rates.

INTRODUCTION

Intra- and interprotein electron-transfer reactions play a crucial role in the energy transduction of all living cells. Electron donor−acceptor distances range from a few angstroms up to 25 Å, and sufficiently fast and efficient electron transfer is achieved by the intervening protein medium.[1,2] Long-range nonadiabatic electron-transfer processes are explained by Marcus' theory, which predicts an exponential process with a rate which depends on a number of parameters:

$$k_{ET} = \frac{2\pi}{\hbar}|H_{DA}|^2(FC) \qquad (1)$$

In the semiclassical model, the driving force (redox potential difference) and the reorganization energy determine the thermodynamic, nuclear, or Franck−Condon factor, FC, whereas the overlap of the donor and acceptor electronic orbitals as well as the orbitals of the intervening medium define the electronic coupling, H_{DA}, which governs the electron tunneling frequency between donor and acceptor and exhibits a roughly exponential distance dependence.[3−5]

$$|H_{DA}|^2 = A^2 \exp[-\beta(r - r_0)] \qquad (2)$$

The role of the intervening medium may be viewed in two different ways. If the actual atomic structure of the protein between the electron donor and acceptor is considered as a network providing various electron-transfer pathways through covalent bonds, hydrogen bridges, or through space jumps (van der Waals contacts), then the optimal pathway, or a set of nearly similar pathways, can be identified by appropriate parametrization.[6] Alternatively, the protein may be considered as condensed matter, with spatially varying packing density, connecting the regions of the donor and the acceptor.[7,8] As the distance between the redox partners increases, the predictions of the two models tend to converge, since the specificity of individual pathways becomes less important.

Electron transfer in nonphotosynthetic redox proteins can be studied with appropriate time resolution using photoactive donors or acceptors, preferably covalently linked to the protein. A large body of such work has been performed using various ruthenium complexes.[5,9−11] An alternative label, TUPS (8-thiouredopyrene-1,3,6-trisulfonate), has also been introduced and its advantageous properties demonstrated.[12] TUPS is capable of acting either as a photoactive electron donor or as a photoactive electron acceptor, depending on the redox partner. We have employed two slightly different chemical forms of the dye for the selective labeling of lysine and cysteine residues in proteins. Cytochrome c was the first protein where the electron transfer between TUPS and the heme was observed.[12] Since its introduction, TUPS has been used to initiate electron transfer in azurin,[13] as well as between cytochrome c and cytochrome c oxidase.[14,15]

The redox properties and the bifunctional nature (oxidant and reductant) of TUPS have been discussed in our recent publication.[16] Here, we re-examine the forward and reverse electron transfers between TUPS and the heme of cytochrome c using the combined techniques of kinetic multichannel and single-wavelength absorption spectroscopy. We demonstrate,

* Corresponding author tel.: +36 62 599 607, fax: +36 62 433 133, e-mail: zimanyi@nucleus.szbk.u-szeged.hu.
[†] Biological Research Center of the Hungarian Academy of Sciences.
[‡] University of Szeged.
[§] Tel Aviv University.
[||] Russian Academy of Sciences.

10.1021/ci050181u CCC: $30.25
Published on Web 10/15/2005

using the combination of the maximum entropy and nonlinear least-squares fits, that the electron transfer between the heme and TUPS exhibits multiexponential kinetics. The distance and directional dependence of the electron transfer is examined by labeling two surface lysines, as well as the two cysteines replacing these lysines by site-directed mutagenesis. Simple preliminary molecular dynamics (MD) calculations provide a likely explanation for both the multiexponential behavior and for the distance dependence of the electron-transfer rates. It appears that the four-ring part of TUPS may occupy several positions close to the protein surface, and the electron in these positions avoids the covalent link via the labeled lysine or cysteine and prefers a through space jump to the surface of the protein instead.

MATERIALS AND METHODS

IPTS (8-isothiocyanatopyrene-1,3,6-trisulfonate) was purchased from Lambda Fluorescence (Austria) and Sigma-Aldrich (Hungary); horse heart cytochrome c and other chemicals were from Sigma-Aldrich.

Construction and Expression of Mutated Cytochrome c. Site-specific mutations were generated by a polymerase chain reaction (PCR) with primers containing the nucleotide changes. Two sequential PCRs were performed to introduce the targeted mutation.[17] The first step was done by the mutagenic and flanking primers, which generated two shorter overlapping sequences, encompassing the region containing the mutation. The full-length fragments were produced in the second PCR step by the two flanking primers, where the overlapping ends of the first amplicons anneal and prime each other's 3′ extension. In addition, the 5′ flanking primer contained a point mutation so that a NcoI restriction endonuclease site was also introduced, allowing the precise insertion of the gene into the expression casette. The full-length fragments were cut by NcoI, phosphorylated by T4 polynucleotide kinase, ligated into the pBAD24 plasmid, digested by NcoI and SmaI restriction enzymes, and dephosphorylated by calf intestine alkaline phosphatase. The plasmid was introduced in the BL21 (DE3) *Escherichia coli* strain for expression of the mutant proteins. Mutations were checked by sequencing the region of interest. The expression and purification of the mutated proteins, as controlled by arabinose induction, was optimized (see Results).

Expression of Recombinant Cytochrome c Proteins. The cells were grown on Superbroth buffer medium at 37 °C until the OD_{600nm} of the culture reached 0.4−0.6 (OD = optical density); then the expression of the target proteins was induced by 0.5−0.8% arabinose, and the culture was incubated further for 12−16 h at 37 °C. Successful expression can be seen after centrifugation from the color of the cell pellet. Cell lysis was carried out by sonication in 50 mM Tris-HCl and a 2 mM EDTA buffer at pH 8.0. Cell debris was removed by centrifugation, and a number of cell specific proteins were salted out from the supernatant by 55% saturated ammonium sulfate solution (351 g/L). Following centrifugation, the salt concentration was reduced by dialysis overnight against a 50 mM sodium phosphate buffer at pH 6.8−7.0. After dialysis, the proteins were loaded onto a column containing Bio-Rex 70 cation-exchange resin, equilibrated with a 50 mM sodium phosphate buffer at pH 6.8−7.0, and eluted with a 50−250 mM NaCl gradient. The salt was exchanged into a 50 mM sodium phosphate buffer by repeated ultrafiltration in Centricon YM-10 filter units.

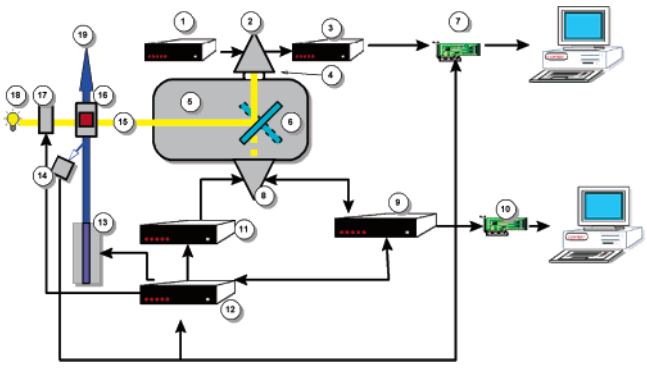

Figure 1. Experimental setup for kinetic spectroscopy. (1) photomultiplier power supply, (2) photomultiplier (Hamamatsu), (3) amplifier, (4) slit, (5) spectrograph/monochromator (Jobin-Yvon HR-320), (6) switching mirror, (7) high-speed digital oscilloscope card (NI5102), (8) diode array detector (PI IRY-512), (9) detector controller (ST120), (10) AT/XT card, (11) gate pulse generator (PG-10), (12) master timer, (13) Nd:YAG laser (Continuum Surelite II), (14) optical trigger, (15) probing light beam, (16) thermostated sample holder, (17) digital shutter (Uniblitz, Vincent Assoc., Rochester, NY), (18) high-pressure xenon lamp (Hamamatsu), (19) actinic light beam.

Preparation of TUPS-Labeled Cytochromes. Cytochrome c was labeled with TUPS at Lys 8 and Lys 39, as described.[12] For labeling of the genetically engineered cysteines, we have slightly modified the published procedure (see also the Results section, below). The thiol-specific TUPS derivative was prepared by incubating IPTS (20 mM) with cystamine (10 mM) at pH 9.0 for approximately 6 h at room temperature. To block IPTS, which did not react with cystamine, lysine was added (final concentration 200 mM), and incubation was performed until IPTS became spectrally undetectable in the solution. Cytochrome c was treated with 5 mM dithiotreitol (DTT) for 1 h to break possible protein dimers formed via disulfide bonds of the engineered cysteines. Excess DTT was removed by gel filtration on a Sephadex G-25 column, equilibrated with a 150 mM N-2-hydroxyethylpiperazine-N′-2-ethanesulfonic acid (HEPES) buffer (pH 8.5). Cytochrome c was incubated with an 8-fold excess of TUPS−cystamine in 150 mM HEPES (pH 8.5)/0.2 M KCl for 4 h at 25 °C. The product was passed through a Sephadex G-25 column and equilibrated with 10 mM HEPES (pH 7.5), to remove salts and nonbound TUPS−cystamine. High-performance liquid chromatography separation and purification was not necessary since the targeted cysteine was the only reactive one, eliminating the possibility of false or multiple labeling.

Kinetic Spectroscopy. A combination of a multichannel and a single-wavelength detector in the same light path (Figure 1) was used for the first time to obtain time-resolved difference spectra (with high spectral resolution and moderate temporal sampling intervals) and absorption kinetic traces at selected wavelengths with fine temporal sampling. TUPS-labeled cytochrome was excited by the third harmonic of a Nd:YAG laser (Continuum Surelite-II, Santa Clara, CA). The energy density of the 355 nm, 5 ns laser pulse at the sample was 20 mJ/cm^2. A continuous white measuring light from a 35 W Hamamatsu high-pressure Xe lamp (Hamamatsu City, Japan), passing the sample perpendicular to the exciting laser light, was dispersed by a Jobin-Yvon spectrograph (HR320,

Longjumeau, France). Two different detectors could be selected by a switching mirror. Multichannel spectroscopy was performed on a gated optical multichannel analyzer (Princeton Instruments IRY512, Trenton, NJ) with submicrosecond time resolution.

Difference spectra were collected at several delays per decade, by averaging 10−20 scans. The spectrum taken at the 1 s delay served as the reference. Single-wavelength absorption kinetic traces were measured at 550 nm with a photomultiplier (Hamamatsu) and digitized at a 20 MHz sampling rate (National Instruments NI5102 oscilloscope card, Austin, TX), and reference traces at 562 nm were subtracted, to obtain the kinetics of heme reduction and reoxidation. Noise suppression of these traces was achieved by averaging over windows of logarithmically increasing width.

All measurements were conducted in a 10 mM HEPES buffer (pH 7.5) at 20 °C. The TUPS−cytochrome concentration was between 10 and 20 μM, the protein was oxidized by substoichiometric addition of cytochrome c oxidase, and oxygen removal was achieved by adding 20 mM glucose, 0.1 mg/mL of glucose oxidase, and 10 μg/mL of catalase.

Data analysis, including the fit of the data matrices by the base spectra of the pure forms, was performed by programs written in Matlab (The Math Works, Natick, MA). The distribution of rate constants and the set of discrete rate constants were determined by the maximum-entropy/nonlinear-least-squares method using the program MemExp-3.0.[18]

Molecular Dynamics and Electron-Transfer Pathway Calculations. The protein database (PDB) entry 1HRC was used for the construction of the models for the TUPS-labeled cytochromes. The MD calculations were carried out with SYBYL 7.0 software (Tripos, Inc., St. Louis, MO) on an Origin2000 workstation (Silicon Graphics, Inc., Mountain View, CA). For the MD simulations, the Tripos force field[19] and a dielectric constant value of 80 were applied, and the cutoff was set to 30 Å for the nonbonding interactions.

Optimal electron-transfer pathways and electron-transfer parameters were calculated by the program HARLEM[20] using the PDB output of the molecular dynamics calculations.

RESULTS

Optimization of the Expression and Purification of Mutated Cytochrome c. In c-type cytochromes, heme cofactors are covalently attached to the polypeptide chain. Heme binding is catalyzed by the enzyme heme lyase during cytochrome c maturation. In our expression system, the corresponding two genes are located tandem in a single plasmid. The casette containing the horse heart cytochrome c (cyc1) gene and the cytochrome c heme lyase (cyc3) gene was cut out from the pBPCYC1(wt)/3 plasmid.[21] For the introduction of the cytochrome c and heme lyase genes, we chose the pBAD24 plasmid, a member of a vector family containing the powerful P_{BAD} promoter of the arabinose operon (*araBAD*). This vector was designed for tight regulation and modulation of protein expression to study the phenotypes of null mutations of essential genes.[22] The plasmid contains an ampicillin-resistance marker gene and the *araC* gene whose product is the positive and the negative regulator of the P_{BAD} promoter. The araC protein is regulated by arabinose sugar; if arabinose is present, the expression from the promoter is turned on; in its absence, the expression occurs at a very low level.[23]

The protein expression was optimized, and the final procedure that was followed is described in the Materials and Methods section. The yields are comparable to the values published,[21] but the reliability of this system in the case of various mutants was better than the other expression methods attempted (data not shown). The purity of the mutated proteins was > 90%, as determined spectrophotometrically and electrophoretically.

Labeling of Mutated Cysteines on the Surface of Cytochrome c by TUPS. The reaction between the amino groups of cystamine and the thiocyano group of IPTS results in the formation of "mono-TUPS-cystamine" and "(di-TUPS)-cystamine" derivatives. With the 2-fold excess of IPTS over cystamine, the latter is dominant, as was demonstrated by simple model calculations (not shown). Previously, IPTS was incubated with a 10-fold excess of cystamine, resulting in only mono-TUPS derivatives. The incubation with cytochrome c, therefore, yielded comparable amounts of the TUPS-labeled protein and the product where the cysteamine half of the label reacted with the protein side chain. When we used a 2-fold excess of IPTS over cystamine, we achieved a much higher percentage of TUPS labeling (∼85%), since both halves of the (di-TUPS)-cystamine are equivalent. After removing the unbound dye, these samples could be used for spectroscopy, since the small fraction of "silent", nonlabeled protein does not interfere with the quality of the data. Further purification of the labeled protein is also possible by ion-exchange chromatography.

Kinetic Absorption Spectroscopy. Electron transfer between TUPS and the heme was first monitored by multichannel spectroscopy. Following the actinic laser pulse, the first excited triplet state of TUPS accumulates and dominates the 300 ns difference spectrum[16] (Figure 2a). Consecutive difference spectra show the appearance of the reduced heme together with the positive radical of TUPS, indicating forward electron transfer, and, eventually, the recovery of the oxidized heme and ground-state TUPS due to reverse electron transfer, as demonstrated by the diminishing features in the millisecond time domain. These difference spectra can be fitted by the spectra of the expected intermediates (Figure 2b), the TUPS triplet minus ground-state spectrum, and the combination of the TUPS positive-radical minus ground-state and the cytochrome reduced minus oxidized difference spectra.

The result of this fit is the time-dependent concentration of the triplet (not shown) and that of the species with the electron temporarily residing on the heme, $TUPS^{+}\sim Fe^{II}$ (Figure 3, symbols). The TUPS triplet base spectrum was measured on a photoexcited TUPS−alanine solution, under oxygen-free conditions and a low enough TUPS concentration to avoid electron self-exchange. The TUPS positive-radical base spectrum was obtained on a similar sample but in the presence of ferricyanide, which oxidizes the excited triplet form of the dye.[16]

Absorption change was also measured at 550 nm using the single-wavelength option, where the characteristic peak of the reduced heme dominates. The properly weighted trace measured at 562 nm was subtracted to eliminate the contribution by the different forms of TUPS. This kinetic trace (Figure 3, black line) overlaps with the concentration kinetics obtained by fitting the multichannel data. The high resolution and high S/N single-wavelength trace is appropriate to study the kinetics of the forward and, especially, the reverse electron-transfer process in detail. A 1 + 1 expo-

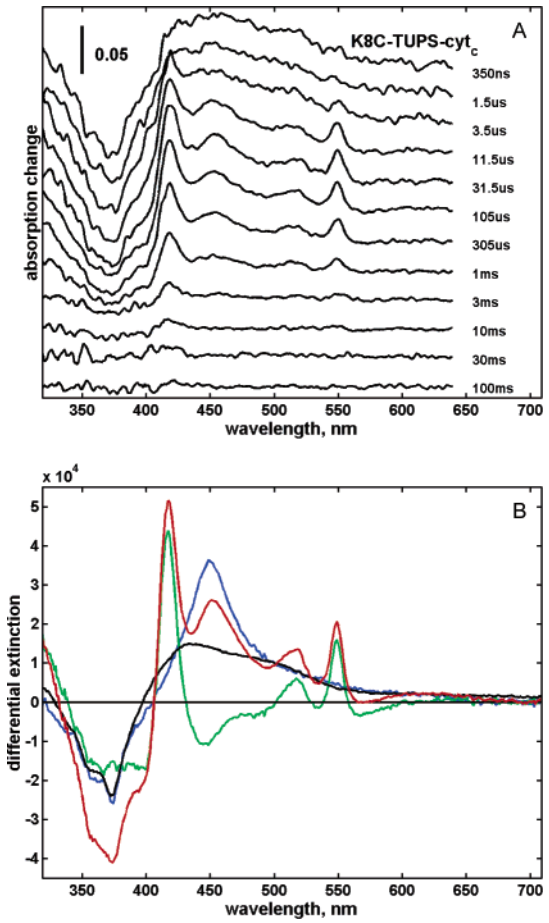

Figure 2. Time-resolved difference spectra at the indicated delays after the actinic laser pulse, measured on cytochrome c and labeled on the genetically engineered cysteine 8 by TUPS (a). Base difference spectra for the fit of the time-resolved spectra: $TUPS^{*T}-TUPS$ (black), $TUPS^{+}-TUPS$ (blue), $cyt_{red}-cyt_{ox}$ (green), and the sum of the latter two (red) (b).

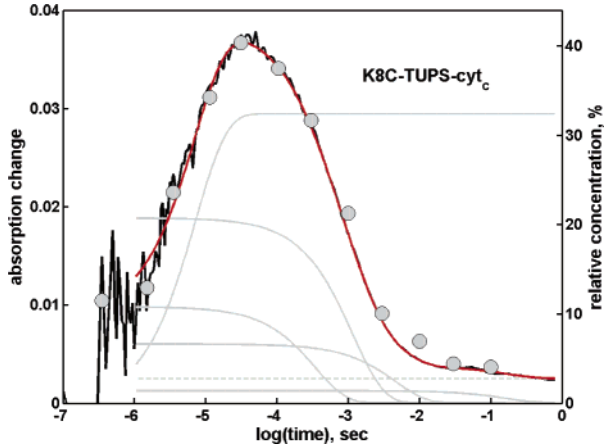

Figure 3. Kinetics of the $TUPS^{+} \sim cyt_{red}$ species from the fit of the time-resolved spectra in Figure 2, expressed as a percentage of the total TUPS-labeled protein concentration (symbols), and the absorption kinetics measured as single-wavelength $\Delta A_{550} - \Delta A_{562}$ (black). Results of the multiexponential fit (red), the individual exponential components (gray), and the baseline (dashed gray).

nential + baseline fit was obviously insufficient (not shown), whereas a 1 + 4 + baseline fit is acceptable (Figure 3, red line).

The maximum entropy method was applied to determine the most probable time-constant distribution that may lead

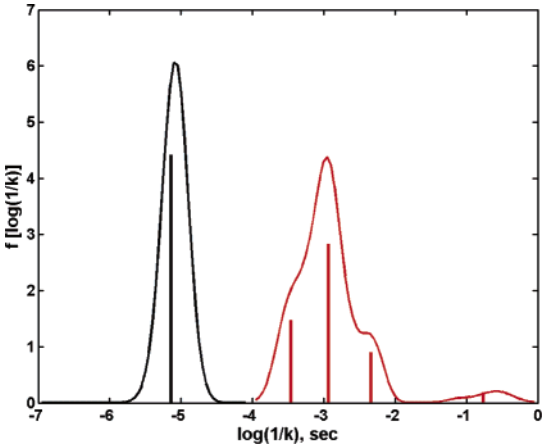

Figure 4. Distribution of time constants for the forward (black) and reverse (red) electron transfer as obtained by the maximum entropy fit of the kinetics in Figure 3. The individual time constants from the multiexponential fit are marked as vertical lines proportional to the corresponding amplitudes.

to the kinetics in Figure 3. The distribution shows a broad peak for the forward electron transfer and four well-resolved peaks for the reverse electron transfer (Figure 4), with a goodness of fit $\chi^2 = 0.966$. The MEM-assisted discrete exponential fit yielded individual rate constants for the exponentials corresponding to the bands in the maximum entropy distribution. The individual exponential components and the baseline are shown in Figure 3 ($\chi_r^2 = 0.806$), and the exponentials are also represented in Figure 4 as lines at the appropriate log(τ) abscissae and with heights proportional to their amplitudes. A similar analysis was also carried out for the K8-, K39-, and K39C-labeled samples, and the results are summarized in Table 1. The latter three samples are characterized by 1 + 3 bands in the maximum entropy distribution, and consequently, the MEM-NLS program recommended 1 + 3 discreet exponentials. One can conclude from the maximum entropy fit that the multiexponential character of the electron transfer between TUPS and the heme is real, and the reverse electron transfer, in particular, cannot be accounted for by a single kinetic phase with a distributed rate constant.

Table 2 lists the geometrical distances for the native lysines, calculated from the crystal structure. The distance to the heme is consistently longer from K8 than from K39. Marcus' theory predicts (eq 2) that the rate constant of electron transfer should be at least 6−12 times faster for K39 with β values ranging from 1.0 to 1.4, even when the smallest difference in the distance to the Fe atom is considered. The more realistic edge-to-edge distance difference predicts at least 2 orders of magnitude rate difference; yet, the electron-transfer rates measured on the K8−TUPS and K39−TUPS samples are only marginally different. The effective reverse electron-transfer rate, calculated as $\sum A_i k_i / \sum A_i$, $i = 2-4$, is 626 and 1113 s^{-1} for K8−TUPS and K39−TUPS, respectively, and the forward rate is even faster for K8−TUPS. It is also obvious that the experimental rates do not conform to the expected distance dependence if the distance is defined along the covalent link between the dye and the protein. The replacement of the lysines by cysteines increases the total covalent bond length to the aromatic part of the dye by one unit. Yet, the measured rates do not decrease ($\sum A_i k_i / \sum A_i = 1269$ and 1116 s^{-1} for K8C−TUPS and K39C−TUPS, respectively).

Table 1. Results of the Multiexponential Fit to the Forward and Reverse Electron-Transfer Kinetics Measured as $\Delta A_{550} - \Delta A_{562}$ on the Four Different TUPS−Cytochrome c Complexes[a]

TUPS-labeled residue		K8	K8C	K39	K39C
rate constants (s^{-1})	k_1	7.95×10^4	1.37×10^5	5.79×10^4	5.26×10^4
	k_2	1525	2878	1642	1554
	k_3	339	852	540	313
	k_4	131	218	92	8
	k_5		6		
	$\langle k \rangle_{decay}$	626	1269	1113	1116
relative amplitudes	A_1	−90%	−77%	−83%	−68%
	A_2	26%	25%	52%	62%
	A_3	59%	49%	43%	27%
	A_4	14%	16%	3%	5%
	A_5		3%		
	baseline	1%	7%	2%	6%

[a] $\langle k \rangle_{decay} = \sum A_i k_i / \sum A_i$ for the decaying phases

Table 2. Geometrical Distances between the End of the Lysine Side Chains and the Heme, Calculated from the Crystal Structure of Cytochrome c

	TUPS-labeled residue	K8	K39
distances, N_Z to ... (Å)	heme Fe	21.3	19.5
	heme edge	15.6	11.4
	heme π-electron system	17.3	15.3

Molecular Dynamics and Electron-Transfer Rate Calculations. Sample heterogeneity is the obvious candidate to explain the multiexponential behavior of electron transfer between TUPS and the heme. This heterogeneity cannot be the conformational heterogeneity (ensemble of conformational substates) of the protein moiety itself, because that is expected to average out at room temperature on the time scale of these electron-transfer processes. For the same reason, a rate constant distribution with a single broad peak is also unlikely at room temperature, as was confirmed by the finding of multiple peaks instead (Figure 4). Therefore, we decided to perform preliminary molecular dynamics calculations to investigate whether the TUPS moiety can occupy several positions relative to the protein moiety, allowed by the rather flexible linker between the two and by the size (geometry) of TUPS. To find such possible conformations, MD calculations were performed on the cytochrome−TUPS system starting from the X-ray structure of horse heart cytochrome c (1HRC.PDB). After connecting the label to Cys 8 (replacing Lys 8 *in silico*), the protein part was positionally restrained, whereas the side chain of the Cys 8 amino acid and all the atoms of TUPS were left freely moving. The cytochrome−TUPS system was energy minimized, and then, 1 ns MD simulations were performed at 300 K using a 1 fs time step. These calculations were started from four different conformations of the dye moiety (Figure 5), and the trajectories of 1 ns MD runs were sampled every 1 ps. No explicit solvent and no periodic boundary conditions were assumed in these calculations, the solvent was modeled by a medium with a dielectric constant of 80 instead. Nevertheless, this preliminary calculation can already show geometrically feasible conformations of TUPS and provide the basis for the qualitative (if not quantitative) interpretation of the electron-transfer rates experimentally obtained.

During the MD simulations, the TUPS moved freely above the surface of the cytochrome initially, and then, it approached the protein surface and occupied several positions. For all MD calculations, the trajectories showed that the label

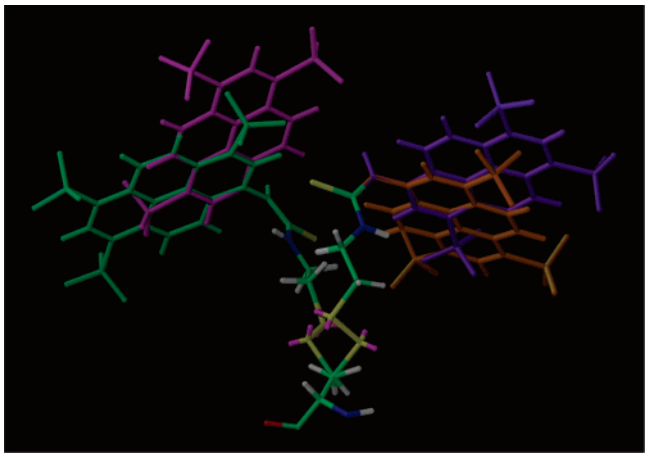

Figure 5. Initial conformations of the TUPS−cysteine moiety for the MD calculations.

spent most of the time in and near these sterically allowed conformational states. Representative frames of these conformations—well after the initial transients—were selected from the trajectories of the MD simulations (Figure 6). It must be noted that there was no interconversion between three of the four stationary conformations, which were, therefore, determined by the initial TUPS conformation assumed.

The first three TUPS positions cluster near one location, whereas the fourth position markedly differs from the other ones. The calculations also yielded less-dominant geometrically possible conformations for the TUPS, which were characterized by shorter dwell times in a certain position compared to the four conformations mentioned above (not shown).

The four dominant structures were tested by the program HARLEM for optimal electron-transfer pathways and electron-transfer parameters (packing density, distance decay factor, and electronic coupling strength) between TUPS and the heme (Table 3). The packing density is a dimensionless parameter varying between 0 and 1, which describes the average packing along all lines connecting the atoms of the donor and acceptor, by considering the fractional length of the lines passing within the van der Waals radius of medium atoms.[24] In these calculations, the electron donor and acceptor were defined as the four-ring aromatic π-electron system of the dye and all atoms contributing to the heme, respectively. The calculations consider nearest edge-to-edge distances. Conformations 2 and 3 appear equivalent in terms of

Table 3. Calculated Electron-Transfer Parameters for the Four Dominant Positions of TUPS Covalently Bound to Cys 8

number of stationary conformation	1	2, 3	4
donor−acceptor edge-to-edge distance, Å	6.83	8.54, 8.33	10.64
packing density between donor and acceptor (ρ, dimensionless)	0.73	0.69, 0.66	0.62
average decay exponent (β,Å^{-1})	1.41	1.50, 1.55	1.61
dimensionless coupling square (H_{DA}^2)	6.38×10^{-5}	2.86×10^{-6}, 2.40×10^{-6}	3.53×10^{-8}

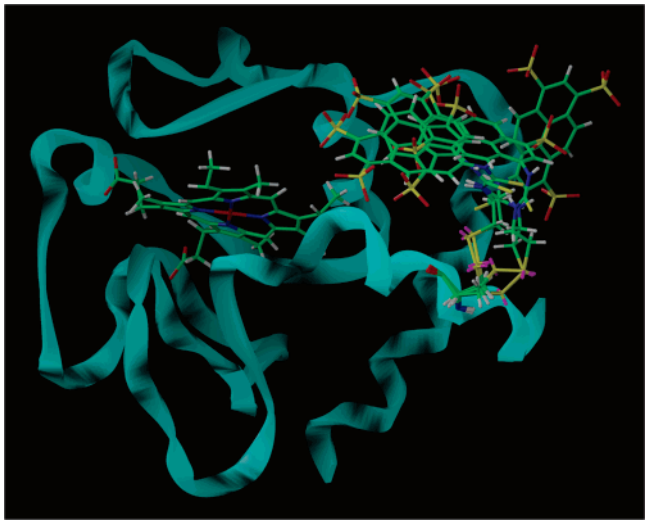

Figure 6. Structure of the representative conformations of TUPS covalently bound to cysteine 8 of cytochrome c. Three out of the four similar locations as well as the one significantly different position are shown.

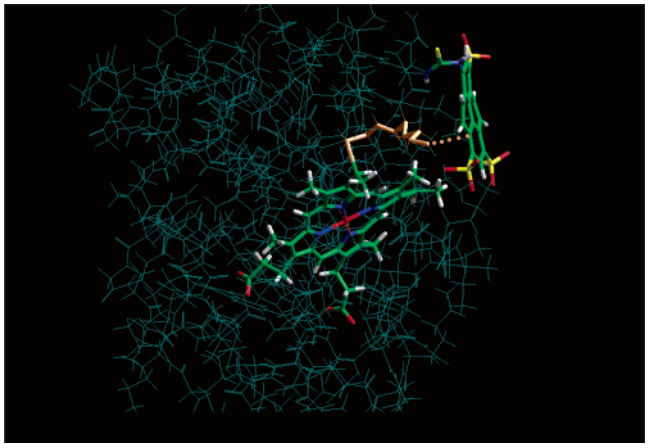

Figure 7. The optimal electron-transfer pathway (gold) calculated for the stationary conformation no. 2 of the K8C−TUPS−cytochrome c system. The electron donor (TUPS) and acceptor (heme) are shown in colored stick representation. The dashed line in the pathway corresponds to the through space jump, and the continuous line corresponds to electron transfer through covalent bonds.

electronic coupling strength; therefore, they are expected to result in very similar electron-transfer rates (eq 1), whereas conformations 1 and 4 are different. The combination of MD and electron-transfer calculations, thus, provide a qualitative explanation for the multiexponential electron-transfer kinetics. It is shown that the geometry of the TUPS-linker moiety allows several distinct positions for TUPS, and they may facilitate substantially different electron-transfer pathways or efficiencies between TUPS and the heme.

One example of the pathway calculations is shown in Figure 7. The electron transfer connecting the edge of TUPS and that of heme starts by a jump to the protein surface and avoids the covalent link via the scaffold of the label and the supporting Cys 8. When the thiouredo carbon atom was selected as the sole source on the electron donor, representing the border of the aromatic part of the dye and the covalent link to the protein, a different optimal pathway was found (not shown). This pathway, however, also includes a through space jump to the protein and, therefore, does not follow the supporting cysteine side chain.

DISCUSSION

It is shown that the photoinduced electron transfer in the TUPS−cytochrome system is more complex than expected on the basis of Marcus' theory. Although the forward electron transfer seems roughly monoexponential at the available signal-to-noise ratio, the reverse electron transfer clearly does not. A straightforward explanation of the multiexponential behavior can be sample heterogeneity. Molecular dynamics calculations, in fact, corroborate this assumption: the TUPS label is likely to occupy several geometrically feasible equilibrium positions at different effective distances from the heme, and the electron may experience different packing densities toward the heme.

Kinetic spectroscopy shows that, in these experiments, there is an initial, unresolved reduction in a small fraction of the hemes (Figure 3). It is not likely that this population corresponds to one of the populations characterized by a certain TUPS conformation, because the forward electron transfer is not supposed to be so fast. One explanation could be the production of solvated electrons by the laser flash, which could rapidly reduce nearby cytochromes, leaving behind the positive radical of TUPS. Such an effect could also explain the finding that a small amount of "permanently" reduced cytochrome seems to accumulate after each laser flash, reflected by the positive baseline necessary to fit the experimental kinetics. These effects are, nevertheless, small enough not to interfere with the major conclusions drawn.

MD calculations suggest that the equilibrium TUPS conformations are not interconvertible under the modeled conditions. Sample heterogeneity can only result in multiexponential electron-transfer behavior if the subpopulations do not mix on the time scale of the electron transfer, because rapid interconversions would lead to a single, average rate constant. For the same reason, protein conformational heterogeneity (substates) is unlikely to result in the observed electron-transfer heterogeneity near room temperature. We must assume that the small number of positions which the TUPS can occupy close to the protein surface are stable enough to define distinct, stationary subpopulations even on the microsecond−millisecond time scale, and the calculated electron-transfer properties are sufficiently different in these subpopulations to qualitatively explain the rate constants found experimentally. We have observed similar multiexponential electron-transfer kinetics on wild-type horse heart

cytochrome c labeled by TUPS on four other lysines, as well as on yeast iso-1 cytochrome c labeled on the native Cys 102. These results will be published elsewhere.

MD calculations were carried out by using the X-ray structure of horse heart cytochrome c 1HRC. This structure was selected because of its high resolution and because it contains the most water molecules (124). There are, altogether, nine available PDB entries on horse heart cytochrome c (excluding its complexes with enzymes), most of them from NMR, but only two others contain water molecules, six each. Two NMR structure files consist of 20 and 40 conformations each, with a certain limited conformational variation. Although all are slightly different from the selected 1HRC structure, the backbone root mean square deviation between 1HRC and the other structures averages 1.88 Å and does not exceed 2.55 Å. Therefore, it is safe to say that 1HRC is a representative cytochrome c structure even in an aqueous medium, and any fluctuations of the protein moiety are substantially smaller than the displacements of the TUPS-linker moiety allowed by its geometry and found by our calculations. For the same reason, the MD calculations aimed at locating possible TUPS positions relative to the protein surface, which are allowed by the covalent link between the two, should at least qualitatively be informative even though the motion of the protein moiety (other than the side chain of Cys 8) was not allowed.

Intraprotein electron-transfer proceeds via covalent bonds, hydrogen bonds, and through space jumps, in this order of efficiency. In certain cases, water molecules filling protein cavities provide a favorable alternative for electron transfer, through hydrogen bridges, to a much lengthier detour through covalent connections. To test this possibility, we have also calculated the optimal electron-transfer pathways for the four MD-calculated TUPS−protein conformations both with the X-ray water molecules included and with filling the structures with water in silico. The best pathways remained the same for all four conformations after including water in either way. In other words, neither the crystal structure water molecules nor the water molecules filling cavities were found in appropriate positions to interfere with the best pathways. This is not surprising because cytochrome c is rather compact and the two redox cofactors are fairly close to each other. The protein packing density was slightly increased by water addition, resulting in better electronic coupling (∼6% increase) and higher expected rate constants (∼13% increase). These changes are, however, negligible when compared to the sensitivity of electron-transfer rates to other factors, such as small variations in distance.

The qualitative picture emerging from our preliminary MD and electron-transfer calculations is promising. It must be noted, though, that the homogeneous dielectric medium is an oversimplification, which emphasizes ionic interactions and neglects possible other factors, such as hydration and solvation effects. More accurate MD calculations are, therefore, planned in explicit water to refine the search for potential stable conformations of the TUPS label covalently linked to cytochrome c.

ACKNOWLEDGMENT

This work was supported by the Hungarian Scientific Research Fund (OTKA T034745, T049207) and by INTAS (011-0002).

REFERENCES AND NOTES

(1) Cramer, W. A.; Knaff, D. B. *Energy Transduction in Biological Membranes. A Textbook of Bioenergetics;* Springer-Verlag: New York, 1990; pp 139−352.

(2) Gray, H. B.; Halpern, J. Distant Charge Transport. *Proc. Natl. Acad. Sci. U.S.A.* **2005**, *102*, 3533.

(3) Marcus, R. A.; Sutin, N. Electron Transfers in Chemistry and Biology. *Biochim. Biophys. Acta* **1985**, *811*, 265−322.

(4) Devault, D. Quantum Mechanical Tunnelling in Biological Systems. *Quart. Rev. Biophys.* **1980**, *13* (4), 387−564.

(5) Gray, H. B.; Winkler, J. R. Electron Tunneling through Proteins. *Quart. Rev. Biophys.* **2003**, *36* (3), 341−372.

(6) Beratan, D. N.; Onuchic, J. N.; Hopfield, J. J. Electron Tunneling Through Covalent and Noncovalent Pathways in Proteins. *J. Chem. Phys.* **1987**, *86* (8), 4488−4498.

(7) Moser, C. C.; Keske, J. M.; Warncke, K.; Farid, R. S.; Dutton, P. L. Nature of Biological Electron Transfer. *Nature* **1992**, *355* (6363), 796−802.

(8) Jones, M. L.; Kurnikov, I. V.; Beratan, D. N. The Nature of Tunneling Pathways and Average Packing Density Models for Protein-Mediated Electron Transfer. *J. Phys. Chem. A* **2002**, *106*, 2002−2006.

(9) Gray, H. B.; Winkler, J. R. Electron Transfer in Proteins. *Annu. Rev. Biochem.* **1996**, *65*, 537−561.

(10) Langen, R.; Chang, I.-J.; Germanas, J. P.; Richards, J. H.; Winkler, J. R.; Gray, H. B. Electron Tunneling in Proteins: Coupling Through a Beta-Strand. *Science* **1995**, *268* (5218), 1733−1735.

(11) Regan, J. J.; Di Bilio, A. J.; Langen, R.; Skov, L. K.; Winkler, J. R.; Gray, H. B.; Onuchic, J. N. Electron Tunneling in Azurin: the Coupling Across a Beta-Sheet. *Chem. Biol.* **1995**, *2* (7), 489−496.

(12) Kotlyar, A. B.; Borovok, N.; Hazani, M. Photoinduced Electron Transfer in Singly Labeled Thiouredopyrenetrisulfonate Cytochrome c Derivatives. *Biochemistry* **1997**, *36* (50), 15828−15833.

(13) Borovok, N.; Kotlyar, A. B.; Pecht, I.; Skov, L. K.; Farver, O. Photoinduced Electron Transfer in Singly Labeled Thiouredopyrenetrisulfonate Azurin Derivatives. *FEBS Lett.* **1999**, *457*, 277−282.

(14) Kotlyar, A.; Borovok, N.; Hazani, M.; Szundi, I.; Einarsdottir, O. Photoinduced Intracomplex Electron-Transfer Between Cytochrome c Oxidase and TUPS-modified Cytochrome c. *Eur. J. Biochem.* **2000**, *267* (18), 5805−5809.

(15) Szundi, I.; Cappuccio, J. A.; Borovok, N.; Kotlyar, A. B.; Einarsdottir, O. Photoinduced Electron Transfer in the Cytochrome c/Cytochrome c Oxidase Complex Using Thiouredopyrenetrisulfonate-labeled Cytochrome c. Optical Multichannel Detection. *Biochemistry* **2001**, *40* (7), 2186−2193.

(16) Kotlyar, A. B.; Borovok, N.; Khoroshyy, K.; Tenger, K.; Zimányi, L. Redox Photochemistry of Thiouredopyrenetrisulfonate. *Photochem. Photobiol.* **2004**, *79* (6), 489−493.

(17) Ausubel, F. M.; Brent, R.; Kingston, R. E.; Moore, D. D.; Seidman, J. G.; Smith, J. A.; Struhl, K. *Current Protocols in Molecular Biology*; Wiley: New York, 1996.

(18) Steinbach, P. J.; Ionescu, R.; Matthews, C. R. Analysis of Kinetics Using a Hybrid Maximum-Entropy/Nonlinear-Least-Squares Method: Application to Protein Folding. *Biophys. J.* **2002**, *82*, 2244−2255.

(19) Clark, M.; Cramer, R. D., III; Van Opdenbosch, N. Validation of the General Purpose Tripos 5.2 Force Field. *J. Comput. Chem.* **1989**, *10*, 982−1012.

(20) Kurnikov, I. V. *HARLEM*; Northwestern University: Evanston, IL. www.kurnikov.org.

(21) Dolgikh, D. A.; Latypov, R. F.; Abdullaev, Z. K.; Kolon, V.; Roder, H.; Kirpichnikov, M. P. Expression of Mutant Genes for Horse Cytochrome c in *Escherichia coli*. *Russ. J. Bioorg. Chem.* **1998**, *24* (10), 756−759.

(22) Guzman, L. M.; Belin, D.; Carson, M. J.; Beckwith, J. Tight Regulation, Modulation, and High-level Expression by Vectors Containing the Arabinose P_{BAD} Promoter. *J. Bacteriol.* **1995**, *177* (14), 4121−4130.

(23) Schleif, R. Regulation of the L-arabinose Operon of *Escherichia coli*. *Trends Genet.* **2000**, *16* (12), 559−565.

(24) Page, C. C.; Moser, C. C.; Chen, X.; Dutton, P. L. Natural engineering principles of electron tunnelling in biological oxidation−reduction. *Nature* **1999**, *402*, 47−52.

CI050181U